Divalent cations activate TRPV1 through promoting conformational change of the extracellular region

Fan Yang,[1] Linlin Ma,[1,2] Xu Cao,[1,3] KeWei Wang,[3,4] and Jie Zheng[1]

[1]Department of Physiology and Membrane Biology, University of California School of Medicine, Davis, Davis, CA 95616
[2]Institute for Molecular Bioscience, The University of Queensland, Brisbane, St Lucia QLD 4072, Australia
[3]Department of Molecular and Cellular Pharmacology, State Key Laboratory of Natural and Biomimetic Drugs, Peking University School of Pharmaceutical Sciences, Beijing 100191, China
[4]PKU-IDG/McGovern Institute for Brain Research, Peking University, Beijing 100871, China

Divalent cations Mg^{2+} and Ba^{2+} selectively and directly potentiate transient receptor potential vanilloid type 1 heat activation by lowering the activation threshold into the room temperature range. We found that Mg^{2+} potentiates channel activation only from the extracellular side; on the intracellular side, Mg^{2+} inhibits channel current. By dividing the extracellularly accessible region of the channel protein into small segments and perturbing the structure of each segment with sequence replacement mutations, we observed that the S1–S2 linker, the S3–S4 linker, and the pore turret are all required for Mg^{2+} potentiation. Sequence replacements at these regions substantially reduced or eliminated Mg^{2+}-induced activation at room temperature while sparing capsaicin activation. Heat activation was affected by many, but not all, of these structural alternations. These observations indicate that extracellular linkers and the turret may interact with each other. Site-directed fluorescence resonance energy transfer measurements further revealed that, like heat, Mg^{2+} also induces structural changes in the pore turret. Interestingly, turret movement induced by Mg^{2+} precedes channel activation, suggesting that Mg^{2+}-induced conformational change in the extracellular region most likely serves as the cause of channel activation instead of a coincidental or accommodating structural adjustment.

INTRODUCTION

Mg^{2+} was the first of many divalent and multivalent cations (such as Ni^{2+}, Gd^{3+}, and polyamines) shown to potently activate transient receptor potential vanilloid type 1 (TRPV1) (Ahern et al., 2005; Riera et al., 2007). It is thought that the potentiation effect of Mg^{2+} on TRPV1 activation may contribute to pain under certain conditions; indeed, intraperitoneal infusion of high concentrations of $MgSO_4$ elicits identifiable pain responses in mice (Gyires and Torma, 1984; Mogil et al., 1999) that are mediated by TRPV1 (Ahern et al., 2005). The effect of Mg^{2+} (as well as other cations such as Ni^{2+}) on TRPV1 gating can be prevented by mutations to two extracellularly located protonation sites in the outer pore region, suggesting that H^+ and divalent cations might affect the same gating machinery (Jordt et al., 2000; Ahern et al., 2005; Luebbert et al., 2010; Wang et al., 2010). Our study described in our companion paper (see Cao et al. in this issue) suggests that Mg^{2+} and another divalent cation, Ba^{2+}, directly affect heat activation while influencing other activation pathways that are allosterically coupled to the C↔O transition of the channel pore. Mg^{2+} lowers the heat activation threshold into the room temperature range, leading to channel activation. In addition, both Mg^{2+} and Ba^{2+} induce channel desensitization to heat but not to capsaicin, suggesting that the divalent cation effect on heat activation is likely limited to the earlier heat-induced conformational change before the opening of the activation gate.

Given the tight linkage between divalent cations and heat activation, it is of great interest to understand how divalent cations interact with TRPV1 protein. Finding the location of channel structures that mediate the divalent cation effect is particularly attractive because numerous regions throughout the channel protein have been implicated to play a role in heat activation (Fig. 1) (Zheng, 2013b). Although allosteric modeling can mathematically describe effects of a stimulus on channel activation and its coupling with other stimuli, it does not provide structural evidence on the location of acting site(s) or the structure(s) transmitting stimulation to the activation gate. Here, we describe experiments aiming at identifying the structures that mediate Mg^{2+} potentiation of TRPV1 activation.

Supplemental Material can be found at:
http://jgp.rupress.org/content/suppl/2013/12/15/jgp.201311024.DC1.html

MATERIALS AND METHODS

cDNA constructs

All constructs used in this study were based on the mouse TRPV1. Six sequence replacement mutants were made at the extracellular regions: three at the S1–S2 linker, one at the S3–S4 linker, and two at the pore turret (as illustrated in Figs. 3, 5, and 7). These mutations were designed to perturb the targeted structures and test their potential involvements in activation gating by Mg^{2+}. For the S1–S2 linker mutations, the first five, middle six, and last six amino acids of the segment ^{456}RPVEGLPPYKLNNTVGD^{472} were replaced with GGGGS, GGGGGS, and GGGGGS, yielding mutant $Rs_1s_2\_1$, $Rs_1s_2\_2$, and $Rs_1s_2\_3$, respectively. For the S3–S4 linker mutation, the segment ^{534}HRKE^{537} was replaced with GGGG, yielding mutant Rs_3s_4. Two more mutants were generated in the pore turret region and were named differently from the previous four. For the first mutant, termed R2, the turret segment ^{613}PPH-KCRGSACRPGN^{626} was replaced with GGGGPGGGGSGGGGS. For the second mutant, termed R3, a longer turret segment, ^{603}GKNN-SLPVESPPHKCRGSACRPGN^{626}, was replaced with GGGGSGGGG-SGGGGS. These are among a group of pore turret mutants that we have studied previously, and their functional properties including heat response are described in a recent report (Cui et al., 2012).

Site-directed fluorescence recordings

Structural changes in the turret and other extracellular regions were monitored with site-directed fluorescence recordings using a patch fluorometry method as described previously (Yang et al., 2010). There are two extracellularly accessible cysteines in mouse TRPV1, C617 and C622, both located in the turret region. For fluorescence resonance energy transfer (FRET) experiments from the turret, we removed the second cysteine with a point mutation, C622A, allowing sulfhydryl-reactive fluorophores to be attached to C617. For FRET experiments from the extracellular S1–S2 linker, we removed both turret cysteines with alanine mutations and then introduced a point mutation, N467C. Functional properties of these cysteine mutant channels are described in a previous report (Yang et al., 2010). Fluorescein maleimide (FM) and tetramethylrhodamine maleimide (TMRM) were used to irreversibly label the cysteine. Fluorescence labeling was performed,
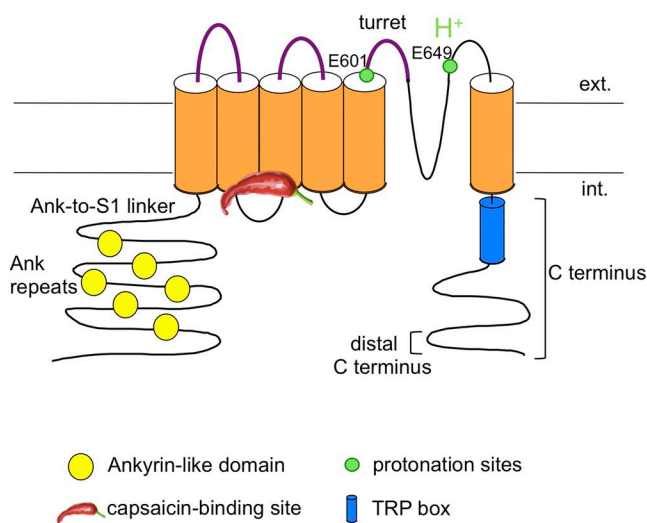

Figure 1. Schematic diagram illustrating the TRPV1 channel topology and highlighting regions previously indicated to be involved in heat and Mg^{2+} activation. Regions tested by mutations in this study are highlighted in purple.

after the establishment of whole-cell patch recording, with an FM/TRMR concentration ratio of 1:1 (1–5 mM in total). The labeling is expected to result in 87.5% of all channels containing both FM and TMRM. Completion of labeling was monitored by patch recording from the time course of change in current amplitude caused by attachment of fluorophores to the cysteine residues (Zheng and Zagotta, 2000). Free fluorophore molecules were thoroughly washed out before fluorescence recording. As multiple FRET pairs may form among fluorophores on the four channel subunits, the measured FRET efficiency reflected the sum of all possible fluorophore couplings and thus did not directly correlate to any single FRET pair (Bykova et al., 2006; Cheng et al., 2007; Zheng, 2013a). FRET changes reflected the overall effect of conformational change at the fluorophore attachment sites on distances between various FRET pairs. Potential contribution of nonspecifically labeled fluorophores was assessed using cells expressing a "cysteine-less" TRPV1 mutant, in which both extracellularly accessible cysteines were mutated to alanine.

FRET between FM and TMRM was measured with the Spectra FRET method (Zheng et al., 2002; Cheng et al., 2007) from voltage-clamped HEK293 cells imaged with an inverted fluorescence microscope (TE2000-U; Nikon) using a 40× oil-immersion objective (NA 1.3). An argon laser (Spectra-Physics) was used to provide the excitation light, with the exposure time controlled by a shutter (Uniblitz; Vincent Associates) synchronized with the camera by software through an amplifier (PatchMaster; HEKA). Two filter cubes (Chroma Technology Corp.) contained the following elements (excitation filter, dichroic mirror, and emission filter): Cube I, Z488/20, Z488rdc, and HQ500LP; Cube II, Z514/10, Z514rdc, and HQ530LP. For Spectra FRET, two spectroscopic images were taken from each cell at each measurement time point, one with the FM excitation at 488 nm using Cube I, and the other with the TMRM excitation at 514 nm using Cube II. From these two images, the total emission spectrum and the TMRM emission spectrum, respectively, were constructed using the linescan function in MetaMorph to determine the fluorescence intensity values along the wavelength axis. Standard emission spectra were collected from cells labeled with only TMRM or FM and used to separate cross-contamination between FM and TMRM caused by spectra overlaps (Takanishi et al., 2006). Spectral measurements were performed with a spectrograph (Acton SpectraPro 2150i; Roper Scientific) in conjunction with a CCD camera (Roper Cascade 128B; Roper Scientific). The sample rate for fluorescence measurements was 1.14 Hz. The rates of photobleaching FM and TMRM by the excitation light were quantified separately from fluorophores attached to the channel and used to correct for photobleaching during FRET experiments.

FRET was quantified from the enhancement of TMRM fluorescence emission caused by energy transfer (Zheng et al., 2002; Cheng et al., 2007) using a method as described previously (Yang et al., 2010), with the following modifications. To assess potential artificial effect of Mg^{2+} on fluorescence emission, Mg^{2+}-dependent changes in fluorescence intensity were measured from cells labeled with either FM or TMRM only. After labeling, the cells were initially bathed in a Na^+-containing solution. After the basal fluorescence level was measured, solutions containing different concentrations of Mg^{2+} were perfused onto the cells while the fluorescence intensity was monitored. For both FM and TMRM, higher Mg^{2+} concentrations increased the fluorescence intensity by very similar fractions. There was no significant difference in the amplitude of Mg^{2+}-induced fluorescence intensity change between FM and TMRM (Mg^{2+} concentrations tested were 10, 30, 100, and 130 mM; P = 0.62–0.97; $n = 6$ each). Therefore, for FM/TMRM intensity ratio measurements, no correction was applied. For FRET efficiency quantification, differences in fluorescence intensity caused by Mg^{2+} were corrected to ensure accuracy. To do so, we estimated the $RatioA_0$ value in the absence and presence of

100 mM Mg^{2+}; FRET efficiency under each condition was calculated using the corresponding $RatioA_0$ value. $RatioA_0$ represents the ratio between TMRM emission intensities (in the absence of FM) upon excitation at the donor and acceptor excitation wavelengths (Erickson et al., 2001; Zheng et al., 2002), and was calculated in the present study at the TMRM peak emission wavelength range (575–590 nm). A particular advantage of quantifying $RatioA_0$ for FRET measurement is that changes in fluorescence intensity caused by many experimental factors (such as the change in Mg^{2+} concentration) can be cancelled out by the ratiometric measurement, just like the TMRM/FM ratio measurement. A similar ratio, termed RatioA, was determined in the presence of FM in the same way as $RatioA_0$. If FRET occurred, the RatioA value should be higher than $RatioA_0$; the difference between RatioA and $RatioA_0$ was directly proportional to the FRET efficiency (Erickson et al., 2001; Zheng et al., 2002). FRET measurements were done with cells that were patch clamped throughout the recording. Mg^{2+}-induced current potentiation and FRET change were recorded simultaneously to allow direct comparing of the time course of structural changes in the fluorophore-labeled region to the time course of channel pore opening.

Cell culture, electrophysiological recordings and associated data analysis, live cell Ca^{2+} imaging and analysis, and temperature control methods are all described in our companion paper (Cao et al., 2013). Electrical measurements were done at +80 mV throughout the study unless otherwise stated. All statistical values are given as mean ± SEM for the number of measurements indicated (n). Statistical significance was determined using Student's t test.

Online supplemental material
Fig. S1 shows the lack of potentiation effect by intracellular Mg^{2+}. Fig. S2 shows capsaicin activation of the extracellular linker mutant channels. The online supplemental material is available at http://www.jgp.org/cgi/content/full/jgp.201311024/DC1.
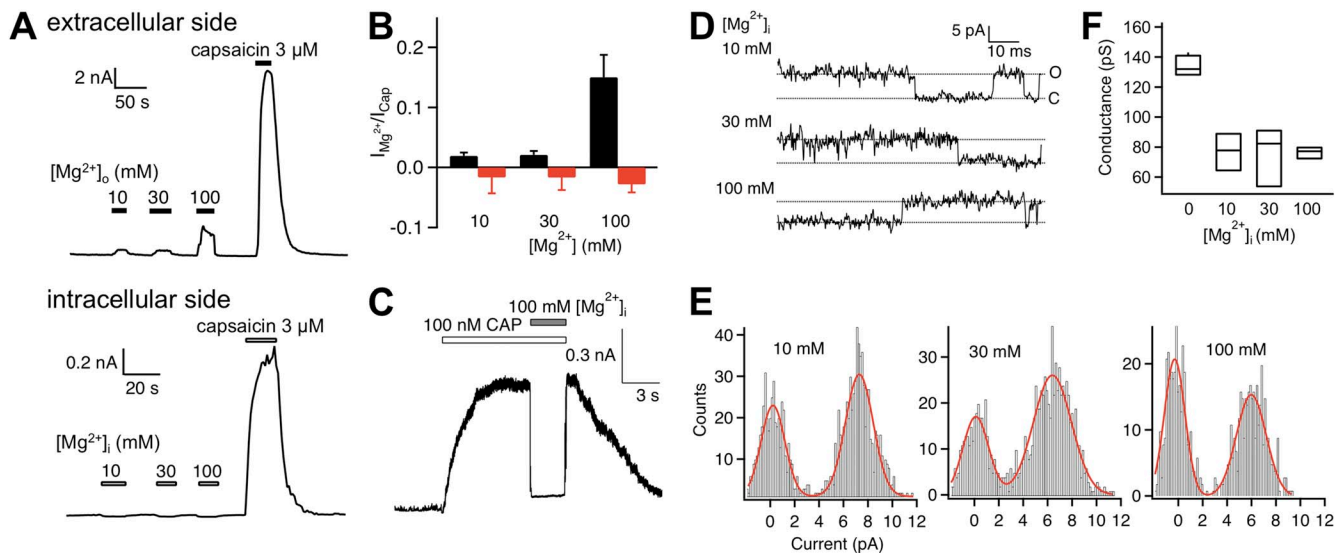
RESULTS

Mg^{2+} potentiates TRPV1 heat activation only from the extracellular side
Experiments described in our companion paper (Cao et al., 2013) were all conducted with extracellular Mg^{2+}. To test whether Mg^{2+} applied to the intracellular side also potentiates TRPV1 heat activation, we repeated these experiments in inside-out patches with various concentrations of Mg^{2+} in the bath. As shown in Fig. 2 A, unlike extracellular Mg^{2+}, intracellular Mg^{2+} failed to elicit a current response from patches that yielded a large current upon capsaicin challenge. Closer inspection showed that intracellular Mg^{2+} inhibited spontaneous channel activity (Fig. S1 A), yielding an overall effect of reducing the current amplitude (Fig. 2 B). We further observed that intracellular Mg^{2+} inhibited capsaicin-induced current (Fig. 2 C; see also Fig. S1 B), which can be largely but not completely explained by an inhibitory effect on single-channel conductance (as described below). Inhibition of capsaicin-induced current could be rapidly and completely reversed upon washing off Mg^{2+} (Fig. 2 C).

We have described in our companion paper (Cao et al., 2013) that extracellular Mg^{2+} inhibits single-channel conductance to partially cover up its potentiation effect on gating. Intracellular Mg^{2+} exhibited a very similar dose-dependent inhibition of single-channel conductance,

Figure 2. Intracellular Mg^{2+} does not potentiate TRPV1. (A) Representative current traces from whole-cell recording at +80 mV with extracellularly applied Mg^{2+} and capsaicin (top) and from an inside-out patch exposed to an increasing amount of intracellular Mg^{2+} and capsaicin (bottom). (B) Summary of the effect of extracellular (black bars; $n = 5$) and intracellular (red bars; $n = 5$–6) Mg^{2+}. (C) Representative current trace demonstrating that intracellular Mg^{2+} blocks, instead of potentiates, current induced by a low concentration of capsaicin. (D) Single-channel current traces recorded at +80 mV in the presence of intracellular Mg^{2+} at the indicated concentrations. (E) All-point histograms of single-channel events at the indicated intracellular Mg^{2+} concentration. The superimposed curve represents a fit of a double-Gaussian function. (F) Box-and-whisker plot of the single-channel conductance versus the corresponding concentration of intracellular Mg^{2+}. The whisker top, box top, line inside the box, box bottom, and whisker bottom represent the maximum, 75th percentile, median, 25th percentile, and minimum value of each pool of conductance measurements, respectively. $n = 3$–4.

reducing the current by $\sim 50\%$ at the 100-mM concentration (Fig. 2, D–F). Even after correcting for conductance inhibition, there is no evidence that intracellular Mg^{2+} activated the channel. Because Mg^{2+} effect on single-channel conductance could be seen from either side of the channel, it is most likely that conductance inhibition occurred because Mg^{2+} ions have a slow permeation rate, leading to blockade of conductance to other permeant ions. Such a permeation block mechanism has been discussed in great detail to explain observations from a wide range of ion channels (Neyton and Miller, 1988; Piasta et al., 2011).

Because Mg^{2+} potentiates TRPV1 only from the extracellular side but not the intracellular side, the channel structure(s) that mediates the potentiation effect should be exposed to the extracellular aqueous environment. To search for the underlying structure(s), we generated systematic sequence alterations in the S1–S2 linker, the S3–S4 linker, and the pore turret, and tested the resultant mutants with extracellular Mg^{2+} using both patch-clamp and live-cell Ca^{2+} imaging recordings. Results from these experiments are described next.

Mutations of the S1–S2 linker can eliminate potentiation effect of extracellular Mg^{2+}

To test for potential involvement of the S1–S2 linker in Mg^{2+}-induced activation, we first replaced the sequence between R456 and D472 with a $(GGGGS)_3$ sequence. However, this mutant construct failed to yield functional current when expressed in HEK293 cells. To circumvent this problem, we divided the S1–S2 linker into three segments and replaced each with a GnS sequence of equal length, where n represents the number of glycine residues (Fig. 3 A). All three constructs yielded functional channels. Resembling many pore turret mutants we studied previously (Yang et al., 2010; Cui et al., 2012), S1–S2 linker mutants exhibited well-preserved capsaicin activation. Accordingly, cells expressing these mutants yielded robust intracellular Ca^{2+} signals upon capsaicin challenge (Fig. 3 B). An example dose–response relationship for $Rs_1s_2\_3$ is shown in Fig. S2. However, although the wild-type channel yielded a strong fluorescence response to 130 mM of extracellular Mg^{2+} that was on average $87.3 \pm 2.7\%$ ($n = 48$) in amplitude compared with that elicited by 10 µM capsaicin, both $Rs_1s_2\_1$
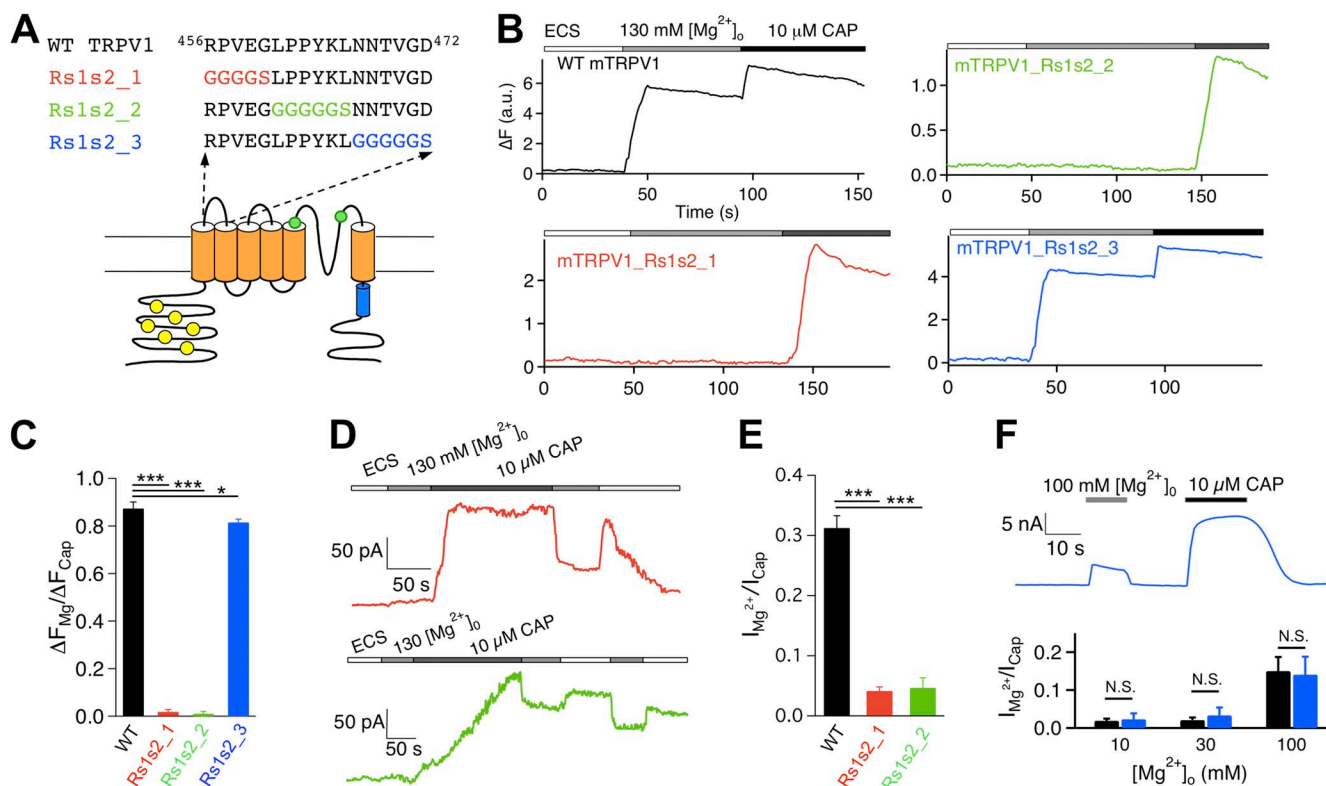
Figure 3. Two out of three S1–S2 linker mutants exhibit a lack of Mg^{2+} potentiation. (A) Diagram illustrating the design of mutations. (B) Representative Ca^{2+} imaging traces. (C) Summary of the amplitude ratio between Mg^{2+}- and capsaicin-induced fluorescence changes in Ca^{2+} imaging experiments. $n = 48$ (wild type), 42 ($Rs_1s_2\_1$), 55 ($Rs_1s_2\_2$), and 89 ($Rs_1s_2\_3$). (D) Representative current traces from $Rs_1s_2\_1$ (top) and $Rs_1s_2\_2$ (bottom) in response to 130 mM Mg^{2+} and 10 µM capsaicin. (E) Summary of the amplitude ratio between 130 mM Mg^{2+}-induced current and 10 µM capsaicin-induced current. $n = 5$ (wild type), 4 ($Rs_1s_2\_1$), and 3 ($Rs_1s_2\_2$). (F) Representative current trace (top) and comparison of the amplitude ratio (bottom) between Mg^{2+}- and capsaicin-induced currents for wild type (black bars) and $Rs_1s_2\_3$ (blue bars). $n = 5$ (wild type) and 3–6 ($Rs_1s_2\_3$). *, P < 0.05; ***, P < 0.001; N.S., not significant.

and $Rs_1s_2\_2$ failed to show a detectable response to Mg^{2+} ($P < 0.001$; $n = 42$ and 55, respectively) (Fig. 3, B and C). For $Rs_1s_2\_3$, a robust response to Mg^{2+} was reliably detected, although the amplitude appeared to be slightly lower than that of the wild-type channel ($P < 0.05$; $n = 89$).

Patch-clamp recordings confirmed the observations from Ca^{2+} imaging experiments, showing a nearly complete absence of Mg^{2+} response from $Rs_1s_2\_1$ and $Rs_1s_2\_2$ but a strong response from $Rs_1s_2\_3$ (Fig. 3, D–F). We also observed that, although a strong capsaicin response could be recorded from both $Rs_1s_2\_1$ and $Rs_1s_2\_2$ after the failed attempt with Mg^{2+}, the capsaicin response was nonetheless slow, which was particularly true for $Rs_1s_2\_2$ ($n = 4$ and 3, respectively) (Fig. 3 D). Recovery from capsaicin activation also appeared to be much slower, allowing us to confirm Mg^{2+} inhibition of the conductance of these mutant channels during the recovery time course (Fig. 3 D). Furthermore, Mg^{2+}-induced current from $Rs_1s_2\_3$ desensitized slowly in the presence of Mg^{2+} (Fig. 3 F), which closely resembled the desensitization behavior of the wild-type channel. In summary, although there are interesting differences in how each S1–S2 linker mutant behaved, the basic observation is

that two of them lost the ability to respond to extracellular Mg^{2+}, whereas the third exhibited a mildly reduced response.

Impaired heat response of the S1–S2 linker mutants

As Mg^{2+} activation and heat activation in the wild-type channel are tightly coupled, we tested how each S1–S2 linker mutant responded to heat. Ca^{2+} imaging recordings demonstrated that, although heating to $40°C$ and higher could elicit a strong fluorescence response from both the wild-type channel and $Rs_1s_2\_3$, the same stimulus failed to elicit a response from cells expressing $Rs_1s_2\_1$ or $Rs_1s_2\_2$ (even though the cells were responsive to capsaicin, confirming positive expression of functional channels) (Fig. 4, A and B). Again, the response of $Rs_1s_2\_3$ to heat is similar but statistically smaller than that of the wild-type channel ($P < 0.05$; $n = 52$).

Results from patch-clamp recordings are consistent with those from Ca^{2+} imaging experiments. As shown in Fig. 4 (C and D), heating to temperatures substantially above the activation threshold of the wild-type channel failed to activate $Rs_1s_2\_1$ and $Rs_1s_2\_2$, whereas capsaicin activated these channels to high open probabilities.
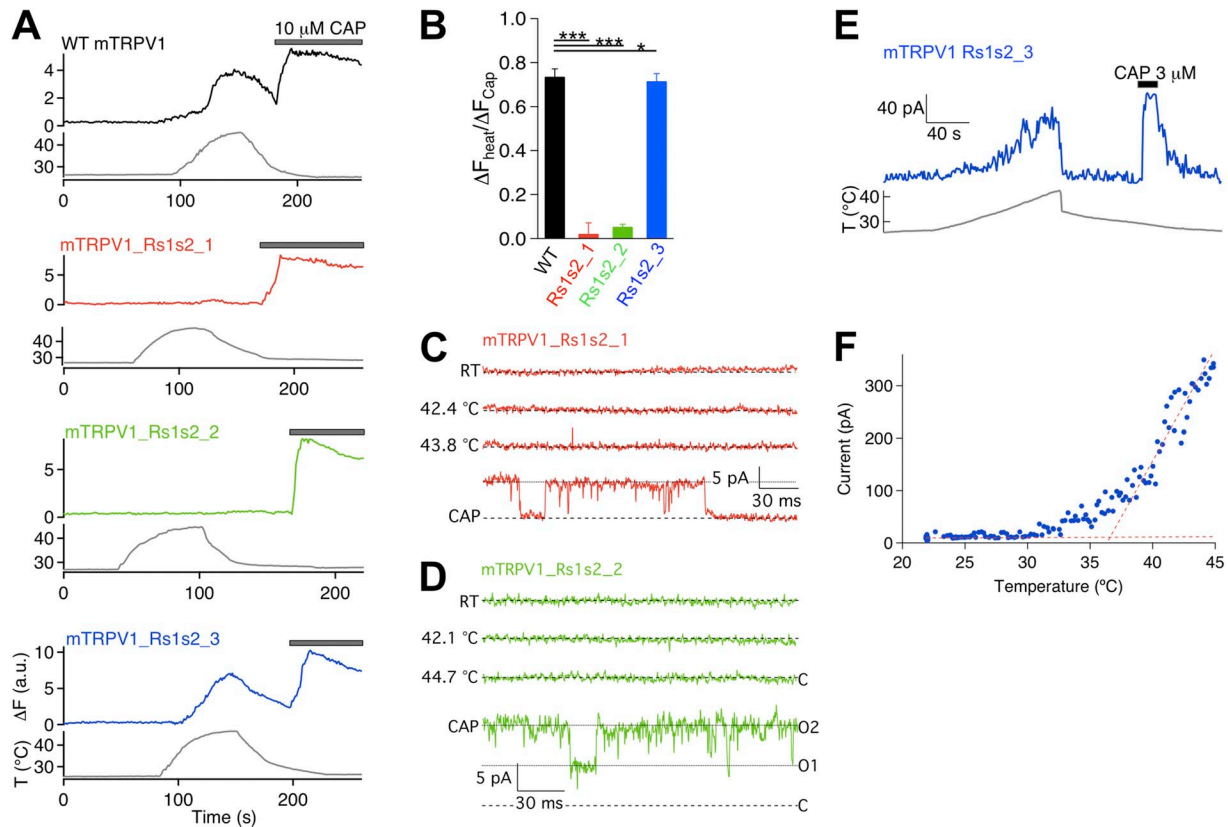
Figure 4. Two out of three S1–S2 linker mutants do not respond to heat. (A) Representative Ca^{2+} imaging traces. (B) Summary of the amplitude ratios between heat- and capsaicin-induced responses. $n = 59$ (wild type), 37 ($Rs_1s_2\_1$), 45 ($Rs_1s_2\_2$), and 52 ($Rs_1s_2\_3$). *, $P < 0.05$; ***, $P < 0.001$. (C and D) Representative single-channel traces recorded at $+80$ mV from $Rs_1s_2\_1$ (C) and $Rs_1s_2\_2$ (D) at room temperature (RT), elevated temperatures, and in the presence of 10 µM capsaicin. The recording shown in D was from a patch containing two channels. (E) Representative current trace recorded from $Rs_1s_2\_3$ in response to heating and 3 µM capsaicin. (F) Current–temperature relationship of $Rs_1s_2\_3$. Dotted lines represent linear fits to the leak and channel currents.
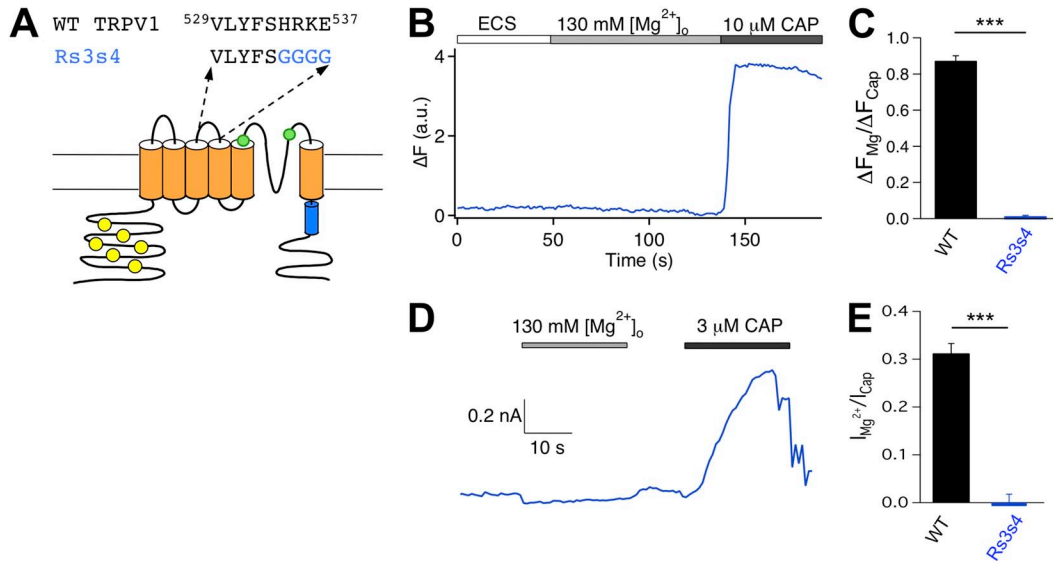
Figure 5. Mutation of the S3–S4 linker eliminates Mg^{2+} response. (A) Diagram illustrating the design of mutation. (B) Representative Ca^{2+} imaging trace. (C) Summary of the amplitude ratio between Mg^{2+}- and capsaicin-induced fluorescence responses for wild type (black bar; $n = 48$) and Rs_3s_4 (blue bar; $n = 65$). (D) Representative current trace recorded at +80 mV in response to 130 mM Mg^{2+} and 3 µM capsaicin. (E) Summary of amplitude ratio between Mg^{2+}- and capsaicin-induced current for wild type (black bar; $n = 5$) and Rs_3s_4 (blue bar; $n = 4$). ***, $P < 0.001$.

In contrast, $Rs_1s_{2\_}3$ was robustly activated by heat (Fig. 4 E). The activation threshold temperature of $Rs_1s_{2\_}3$ was estimated at $36.9 \pm 0.7°C$ ($n = 6$), which is close to the $37.7 \pm 0.3°C$ ($n = 9$) value for the wild-type channel ($P > 0.05$).

In summary of all results from the S1–S2 linker mutants, we found that the first two thirds of the linker is required to support both Mg^{2+} and heat activation, and the last one third appears to have a minor role in both activation forms.

Mutation of the S3–S4 linker eliminates Mg^{2+} activation but spares heat activation

We next examined the Rs_3s_4 mutant (Fig. 5 A). Both Ca^{2+} imaging and patch-clamp recordings showed that this mutant lost Mg^{2+}-induced activation but remained sensitive to capsaicin challenge (Fig. 5, B–E, and Fig. S2). Based on the close correlation between Mg^{2+} activation and heat activation observed from the S1–S2 linker mutants, we anticipated that Rs_3s_4 would also show a lack of
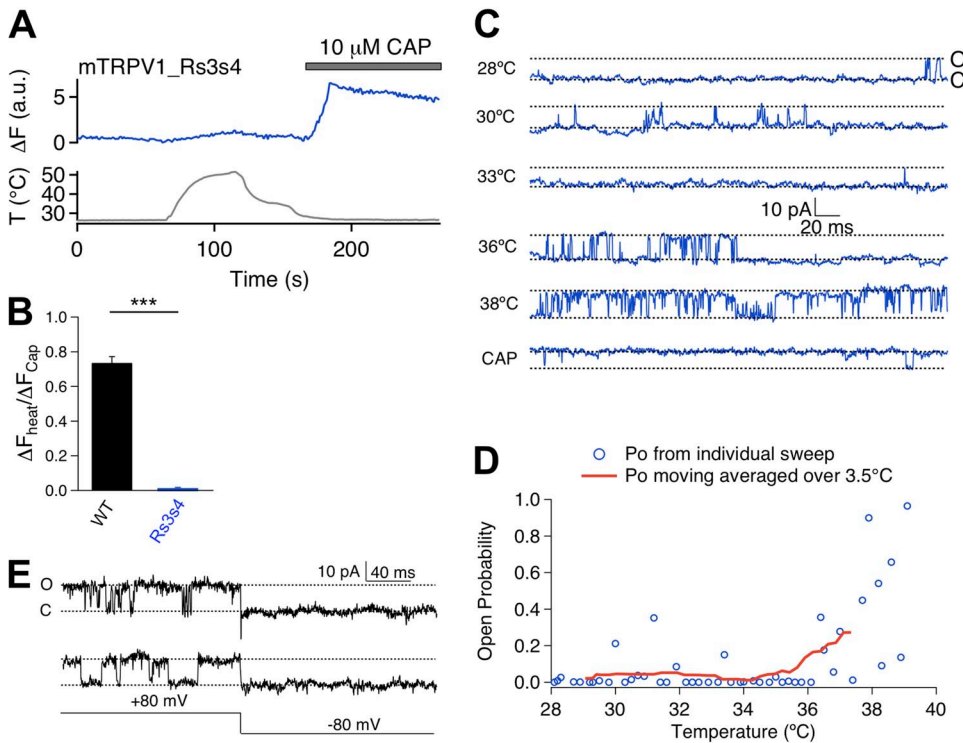

Figure 6. Rs_3s_4 mutant exhibits heat-induced current activation. (A) Representative Ca^{2+} imaging trace (top) upon heat (bottom) and capsaicin challenges. (B) Summary of amplitude ratio between heat- and capsaicin-induced currents for wild type (black bar; $n = 59$) and Rs_3s_4 (blue bar; $n = 55$). ***, $P < 0.001$. (C) Representative single-channel traces recorded at +80 mV at varying temperatures and in the presence of 3 µM capsaicin. (D) Relationship between open probability (P_o) and temperature. Open circles represent average P_o of individual sweeps, and the red trace represents average P_o over a 3.5°C range. (E) Representative single-channel traces demonstrating rapid deactivation transition upon voltage step from +80 to −80 mV.

heat sensitivity. Indeed, Ca^{2+} imaging experiments showed that heating up to near 50°C barely induced any fluorescence signal at the resting membrane potential from cells expressing Rs_3s_4 (Fig. 6, A and B). Surprisingly, patch-clamp recordings at +80 mV showed that this mutant channel could be activated by heat (Fig. 6 C), with the activation threshold temperature being apparently similar to that of the wild-type channel (Fig. 6 D). We also observed that, although the channel could be activated to high open probabilities, this was only observed at a depolarized voltage of +80 mV. Upon repolarizing to −80 mV, the heat-activated channel promptly closed (Fig. 6 E). This rapid deactivation behavior resembles that of the wild-type channel (see, for example, Voets et al., 2004). It thus appears that Rs3s4 remains heat sensitive. Reasons for the lack of a fluorescence signal are unclear. Because the voltage-dependent process has a substantial influence on channel activation when the heat activation pathway is potentiated, one possibility for the lack of a fluorescence response in live cells may be associated with the negative resting membrane potential under our experimental condition that might keep this mutant channel in the closed state. In summary,

mutation at the S3–S4 linker eliminates Mg^{2+} activation but not heat activation. The fact that heat can activate Mg^{2+}-insensitive mutant channels indicates that the two gating modalities may be supported by only partially overlapping channel structures.

Mutations in the pore turret simultaneously affect Mg^{2+} and heat activations

We applied the same strategy to test potential involvement of the pore turret in Mg^{2+} activation (Fig. 7 A). The pore turret has been shown to participate in heat activation; several turret mutants exhibited diminished heat response (Yang et al., 2010; Cui et al., 2012). One such turret mutant, R3, was found to also exhibit a near complete absence of Mg^{2+}-induced fluorescence signal (Fig. 7, B and C). Patch-clamp recordings further showed that Mg^{2+} barely elicited any current from R3-expressing cells that responded strongly to capsaicin (Fig. 7, D–F). Similarly, Ba^{2+} also failed to activate R3 (Fig. 7, G–I). These findings were further supported by observations from a less severe turret mutant, R2. Like R3, R2 exhibited substantially reduced Mg^{2+}-sensitive fluorescence signals (Fig. 7, B and C). In addition, both Mg^{2+} and
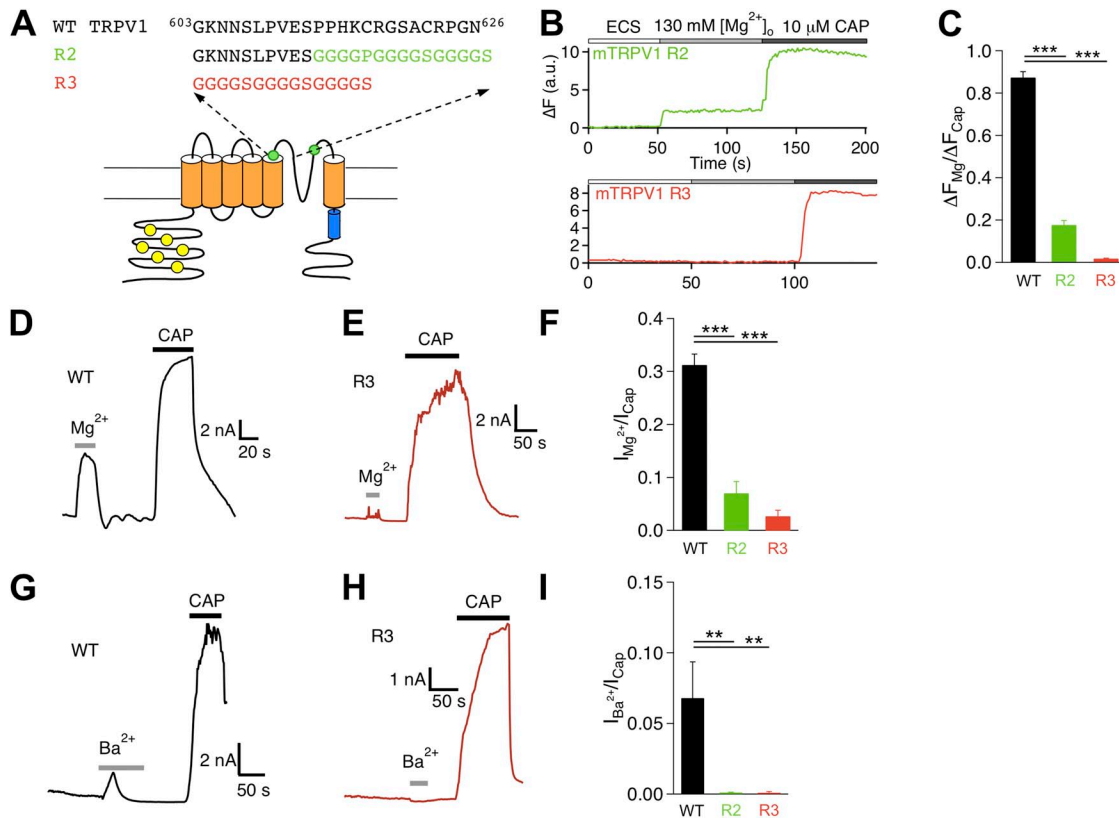

Figure 7. Pore turret mutants exhibit diminished Mg^{2+} response. (A) Diagram illustrating the design of mutations. (B) Representative Ca^{2+} imaging traces. (C) Summary of amplitude ratio between Mg^{2+}- and capsaicin-induced fluorescence responses. $n = 48$ (wild type), 38 (R2), and 66 (R3). (D and E) Representative current trace of wild type (D) and R3 (E) challenged by Mg^{2+} and capsaicin. (F) Summary of amplitude ratio between Mg^{2+}- and capsaicin-induced currents. $n = 5$ (wild type), 9 (R2), and 5 (R3). (G and H) Representative current trace of wild type (G) and R3 (H) challenged by Ba^{2+} and capsaicin. (I) Summary of amplitude ratio between Ba^{2+}- and capsaicin-induced currents. $n = 5$ (wild type), 6 (R2), and 4 (R3). **, P < 0.01; ***, P < 0.001.

Ba^{2+} induced a much smaller current from R2 than the wild-type channel (Fig. 7, F and I). Clearly, the pore turret mutants that affected heat activation also significantly diminished divalent cation–induced activation.

Extracellular Mg^{2+} promotes turret conformational change

Heat activation of TRPV1 involves turret movement that can be directly observed from changes in FRET between fluorophores attached to the turret (Yang et al., 2010). If Mg^{2+} promotes heat activation, can Mg^{2+} induce turret movement in the absence of a temperature change? To answer this question, we performed patch fluorometry measurements (Fig. 8 A). FM and TMRM were attached to C617 in the middle of the turret (after removing another turret cysteine by a C622A mutation). Similar to the wild-type channels, fluorophore-labeled channels were reversibly potentiated by Mg^{2+} at room temperature, which can be seen by patch-clamp current recordings (Fig. 8 B, open circles; $n = 14$). The ratio between TMRM and FM fluorescence intensities was also increased by Mg^{2+}, with the change being reversible upon removal of Mg^{2+} (Fig. 8 B, red circles). An increase in the TMRM/FM intensity ratio indicated an increase in FRET, suggesting that the fluorophores moved closer to each other, just like when heat was used to activate the channel (Yang et al., 2010). In addition, an "overshoot" in the TMRM/FM ratio was often observed at the end of the raising phase; upon removal of Mg^{2+}, an increase in the TMRM/FM ratio was also often seen before the

fluorescence decline phase (Fig. 8 B). As a negative control, the TMRM/FM ratio of untransfected cells was monitored under the same experimental conditions but was found to be completely insensitive to changes in Mg^{2+} concentration (Fig. 8 C). Thus, the observed changes in the TMRM/FM ratio at C617 indicate that Mg^{2+} induced a turret movement at room temperature, and the movement likely proceeded in multiple steps.

To further confirm that changes of the TMRM/FM ratio at the pore turret reflected Mg^{2+}-induced conformational changes, we repeated the patch fluorometry experiment with a mutant channel whose two turret cysteines were removed, and a new cysteine was introduced into the S1–S2 linker at N467, the first amino acid of the Rs$_1$s$_2$_3 mutation. Because the Rs$_1$s$_2$_3 mutant channel responded to Mg^{2+} similarly to the wild-type channel, it is likely that the structure near N467 does not participate in Mg^{2+}-induced structural changes. Indeed, we found that the application of Mg^{2+} failed to induce any detectable change in the TMRM/FM ratio, even though the labeled channels could be substantially activated by Mg^{2+} like the wild-type and Rs$_1$s$_2$_3 channels (Fig. 8 D; $n = 6$). Furthermore, when the experiment was repeated with channels missing both turret cysteines, we again observed Mg^{2+}-induced channel activation, but the background fluorescence did not change (Fig. 8 E; $n = 3$). These negative control experiments confirmed that the observed fluorescence changes at the pore turret are caused by Mg^{2+}-induced conformational change.
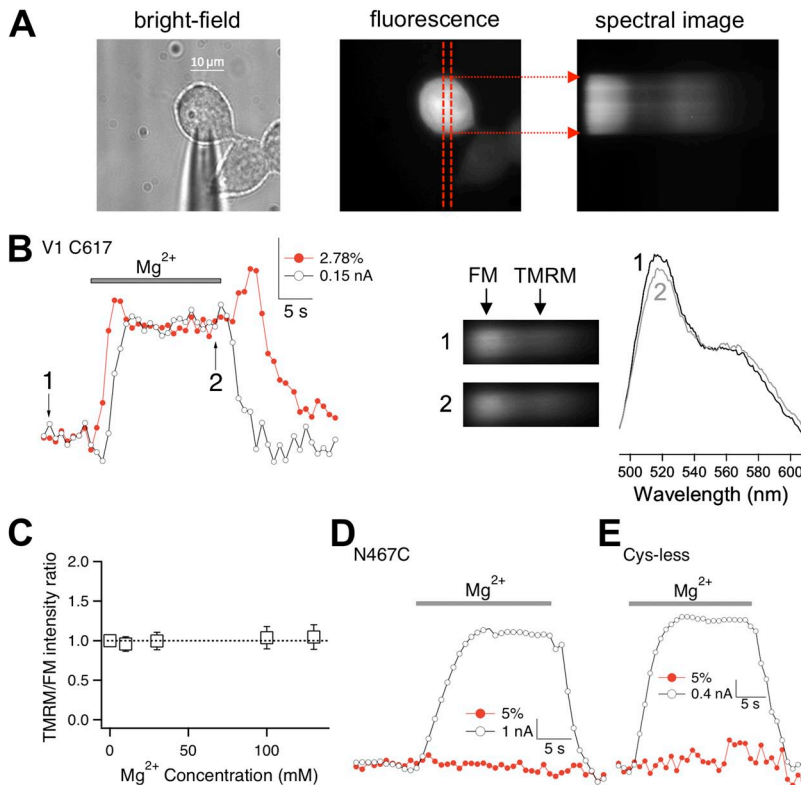
Figure 8. Mg^{2+} induces pore turret movement. (A) Bright-field and fluorescence images of a patch-clamped fluorescently labeled cell. Red dashed lines mark the position of the spectrograph input slit. Fluorescence signal from the area covered by the slit was collected by spectral imaging (right). (B; left) Simultaneous recordings of current (open circles) and TMRM/FM fluorescence intensity ratio (red circles) upon the application of 130 mM Mg^{2+}. (Right) Spectral images and spectra taken at time points 1 and 2 labeled in the left panel. (C) Control experiments with untransfected cells labeled with FM or TMRM ($n = 6$ each). No change in relative fluorescence intensity could be detected when various concentrations of Mg^{2+} were added. (D) Fluorescence signal recorded at N467C (which is close to the end of the S1–S2 linker) did not change upon Mg^{2+}-induced activation. (E) Background fluorescence did not change upon Mg^{2+}-induced activation of mutant channel without any extracellularly accessible cysteine.

One important observation from the FRET experiments was that the Mg^{2+}-induced FRET change at the pore turret preceded the current change that reflected the final opening of the ion-conducting pathway (Fig. 8 B). This sequential order is reminiscent of a similar sequential order of the gating current from voltage-sensor movements and the open-channel ionic current seen in voltage-gated channels (Sigworth, 1994; Bezanilla, 2008). The phenomenon thus suggests that in TRPV1, the turret moved before channel opening. Upon removal of Mg^{2+}, the FRET signal first showed a transient increase that coincided with channel closure, followed by a lagging slow decrease when the channel was already closed (Fig. 8 B). Overall, the change in fluorescence signal upon channel closure showed a reversed sequence compared with that upon channel opening. The observation that Mg^{2+}-induced turret movement preceded channel opening strongly suggests that Mg^{2+}-induced movement in the turret (and likely other extracellular regions that participate in Mg^{2+} potentiation) promotes channel activation.

Mg^{2+}-induced turret movement is less substantial than heat-induced movement

To compare Mg^{2+}-induced turret conformational change to that induced by heat, we used the Spectra FRET method to quantify changes in FRET efficiency caused by turret movement (Fig. 9). We found that the magnitude of Mg^{2+}-induced FRET change is smaller than that of heat-induced FRET change at the same turret position (Fig. 9 C), which is consistent with the observation that Mg^{2+} only partially activated TRPV1 (see, for example, Fig. 3 of our companion paper, Cao et al., 2013). As anticipated from a separation of the capsaicin and heat activation pathways, capsaicin failed to induced any FRET change at the pore turret (Fig. 9 C; $n = 5$) where heat and Mg^{2+} induced positive FRET changes. In agreement with the TMRM/FM ratio measurements, there was no change in FRET efficiency at N467C or from the background fluorescence (Fig. 9 C; $n = 3–6$).

DISCUSSION

Our results demonstrate that most of the extracellular channel regions are required to support Mg^{2+} potentiation of TRPV1 activation. Participation of the channel's extracellular regions in activation gating is not surprising, as mutations and H^+ binding to many extracellular sites have been found to have strong and often specific gating effects (Jordt et al., 2000; Myers et al., 2008; Grandl et al., 2010; Boukalova et al., 2013), and we have shown previously that the pore turret undergoes a substantial and specific conformational change during heat activation (Yang et al., 2010; Cui et al., 2012). What came as a surprise is how widely spread the participating regions are for Mg^{2+} potentiation. Whether all the participating

regions are involved in the activation conformational change remains to be determined. The lack of a fluorescence change at the S1–S2 linker site (N467C) suggests that perhaps some of the peripheral regions might provide structural supports but do not directly participate in the Mg^{2+}-induced conformational change. If this is the case, it is most likely that the extracellular linkers and the pore turret interact with each other. More importantly, the mutational effects on Mg^{2+} potentiation at extracellular linkers and the direct evidence of turret movement from the FRET experiments suggest that Mg^{2+} induces a substantial conformational rearrangement of the channel's extracellular structures that leads to channel activation.

The sidedness of Mg^{2+} potentiation effect

An important finding of this study is that Mg^{2+} potentiates heat activation only from the extracellular side but not from the intracellular side. Given its small size and high solubility in water, Mg^{2+} should be in direct contact with any channel structure that is exposed to the aqueous environment. Should an intracellular channel structure undergo a large conformational change during
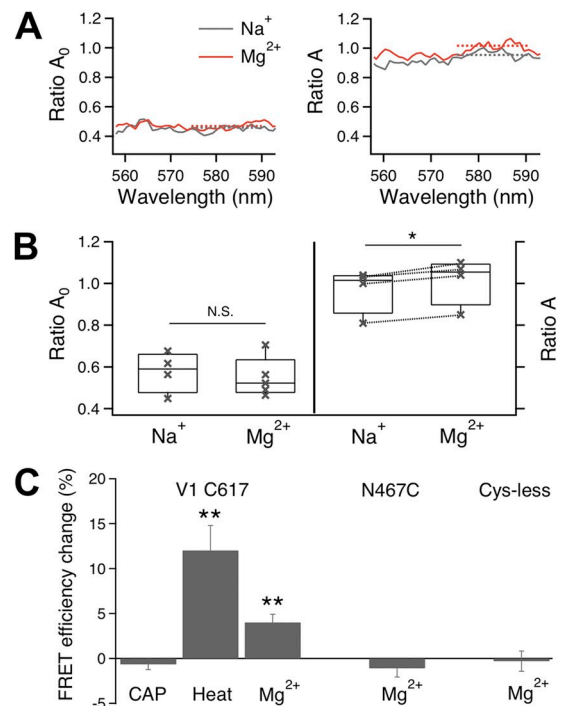

Figure 9. Mg^{2+} induced FRET changes at the pore turret. (A) Mg^{2+} did not affect $RatioA_0$ of TMRM-labeled cells (left) but increased RatioA of FM/TMRM-labeled cells (right), indicating an increase in FRET efficiency. (B) Statistical analysis of Mg^{2+} effects on $RatioA_0$ (left) and RatioA (right). Dotted lines on the right link measurements from the same cells; $RatioA_0$ measurements were not paired. (C) Summary of Mg^{2+}-induced changes in FRET efficiency, which is defined as the FRET efficiency values in the presence of 100 mM Mg^{2+} subtracted by the FRET efficiency value in the presence of Na^+. *, P < 0.05; **, P < 0.01. $n = 3–6$.

activation, having high millimolar concentrations of Mg^{2+} in the surrounding solution is expected to exert an energetic influence on the stability of these conformations (Fersht, 1998), which is likely to be reflected by changes in channel activation. An excellent demonstration of this effect is that changes in ionic strength of the bath solution substantially affect voltage-sensor movement via the solvent-accessible cavities near S4 (Islas and Sigworth, 2001). Because the "heat sensor" of TRPV1 is expected to undergo a large conformational transition upon temperature change (Clapham and Miller, 2011), should it be exposed to the intracellular side of the channel, it would likely allow intracellularly applied Mg^{2+} to affect heat activation. Therefore, out results suggest that heat-induced conformational changes to intracellular channel structures might be either minimal or limited to mostly buried protein structures.

Structural considerations of Mg^{2+}-induced TRPV1 activation

The structural architecture of TRPV1 is generally assumed to resemble that of the voltage-gated potassium channels, for which crystallographic studies revealed that the four turrets pose around the pore, the S1–S2 linkers locate near the turrets (with the S1 end pushing against the turret), and the S3–S4 linkers locate peripherally (Long et al., 2005, 2007) (Fig. 10 A). A low resolution cryo-EM study supports the anticipated structural

similarity between TRPV1 and voltage-gated potassium channels (Moiseenkova-Bell et al., 2008). In potassium channels, the direct contact between the top of S1 and the pore region plays a critical role in voltage-dependent gating, perhaps by providing support for the voltage sensor to exert force onto the activation gate through the S4–S5 linker (Lee et al., 2009). Here, we observed in TRPV1 that the first two thirds of the S1–S2 linker (presumably in close proximity to the pore turret) and the turret itself are required to support Mg^{2+} and heat activation, whereas mutations in the likely peripherally located S3–S4 linker and the S2 end of the S1–S2 linker only affected Mg^{2+} activation or had minor effects on gating, respectively. These results agree with the existence of an overall structural similarity between TRPV1 and voltage-gated potassium channels (Fig. 10 B).

Observations described here and in our companion paper (Cao et al., 2013) indicate several gating steps during TRPV1 activation that are summarized in a schematic diagram shown in Fig. 10 C. Divalent cations cause a conformational rearrangement specifically to extracellular structures. This conformational rearrangement can be directly observed from the turret region with site-specific fluorophore labels, and can be disrupted by mutations to the turret as well as extracellular linkers between transmembrane helixes. At least for the pore turret, the conformational change precedes pore opening, suggesting a likely cause–effect relationship. If
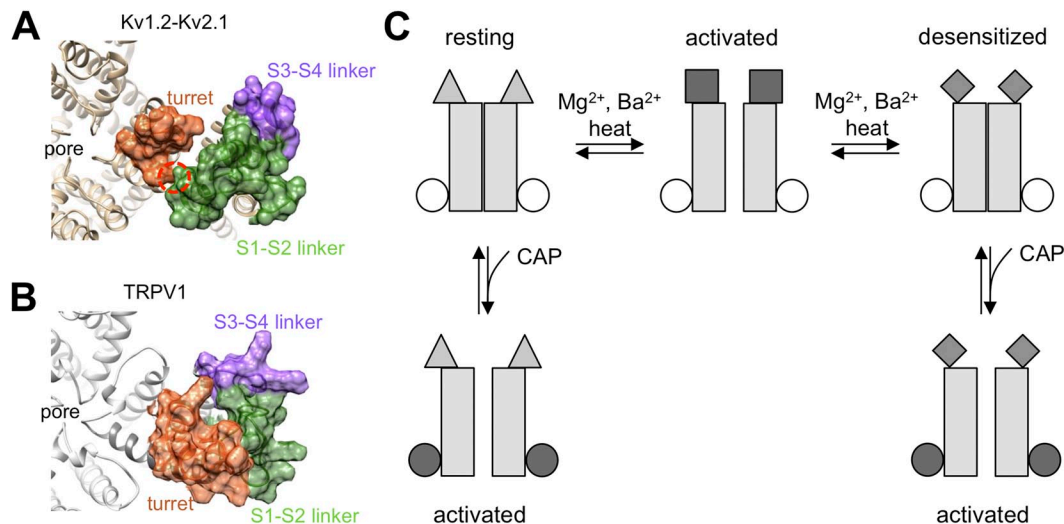

Figure 10. Divalent cations activate TRPV1 through conformational changes of the extracellular region. (A) Crystal structure of the Kv1.2-Kv2.1 chimera (Protein Data Bank accession no. 2R9R), with the pore turret, S1–S2 linker, and S3–S4 linker highlighted in surface-plot mode in different colors. The red circle highlights the S1–turret interaction that supports voltage-dependent gating. (B) Rosetta-generated structural model for TRPV1. (C) Schematic diagram summarizing the gating process of TRPV1 by divalent cations, heat, and capsaicin. Mg^{2+}/Ba^{2+} and heat work from the extracellular side to induce a conformational rearrangement of channel structures exposed to the aqueous environment, which is coupled to pore opening (first horizontal transition). In the presence of Mg^{2+}/Ba^{2+} or heat, the extracellular structure settles down over time to a more stable conformation that does not support the open pore conformation, leading to desensitization (second horizontal transition). Capsaicin binding to the intracellular S2–S3 linker region also leads to pore opening. This can happen to resting channels (left vertical transition) as well as to channels already desensitized to divalent cations (right vertical transition).

the stimulation by divalent cations or heat lasts long enough, a Ca^{2+}-independent conformational arrangement occurs, causing the channel to be desensitized to both divalent cations and heat. Although little is known about the nature of the desensitization process, we speculate that it is not caused by the closure of the activation gate (because capsaicin can still activate the desensitized channel). Instead, it may occur to the same channel structures that are affected by heat and divalent cations and are coupled to the activation gate. Capsaicin-induced activation is largely isolated from these extracellular processes and can proceed from either the resting state or the desensitized state. Details of these gating steps remain to be elucidated in future investigation of the heat activation mechanism.

How do divalent cations potentiate TRPV1 heat activation? Although the study described in this and in our companion paper (Cao et al., 2013) identifies the pathway and channel structures that support the gating effects of divalent cations on TRPV1, the physical process underlying divalent cation–induced activation remains unclear. Several possibilities are considered briefly here. Based on observations that removing two extracellularly exposed proton-binding sites can eliminate the gating effect of many cations such as Mg^{2+}, Ni^{2+}, Ca^{2+}, Gd^{3+}, and polyamines (Ahern et al., 2005, 2006; Tousova et al., 2005; Ohta et al., 2008; Luebbert et al., 2010), it has been generally assumed that these cations bind to the same two sites. Proton binding to TRPV1 exerts a strong potentiation effect on gating that brings the open probability to apparently quite high levels (Tominaga et al., 1998; Jordt et al., 2000). The two major proton-binding sites, E601 and E649 (corresponding to E600 and E648, originally identified in rat TRPV1) (Jordt et al., 2000), are both in the outer pore region (see Fig. 1). E601 is located at the junction between the S5 transmembrane domain and the pore turret, and E649 is located at the outer mouth of the pore near the selectivity filter. It can be envisioned that the binding of positive charges (H^+, Mg^{2+}, or other cations) at these positions may exert a substantial influence on the conformation of the channel pore or the surrounding outer pore structures such as the turret. In this scenario, the peripheral extracellular structures might play a supporting but nonetheless necessary role similar to what S1 does in potassium channels.

There are, however, noticeable differences between proton and divalent cations in potentiating TRPV1 activation. First, in all the mutant channels we tested, the two proton-binding sites remained unaltered. So to fit results from this study to the proton-binding site hypothesis, one has to assume that mutations in the broad extracellular regions altered the structure at the proton-binding sites so that Mg^{2+} can no longer bind there, or its binding fails to exert the same gating effect. Second, although the binding of H^+ to the two outer pore

sites occurs at micromolar concentrations (pH 6), we observed that it takes at least 10 mM Mg^{2+} to generate a detectable gating effect. In addition, no evidence for saturation of the potentiation effect was observed even at a concentration of 130 mM. Previous studies with Mg^{2+} (Ahern et al., 2005; Riera et al., 2007; Wang et al., 2010), Ca^{2+} and Sr^{2+} (Ahern et al., 2005), and Ni^{2+} (Luebbert et al., 2010) all yielded similar results. Only 30 µM Gd^{3+} and 500 µM spermine exhibited detectable gating effects at submillimolar concentrations at room temperature (Tousova et al., 2005; Ahern et al., 2006). Nonetheless, potentiation by polyamines does not always require the proton-binding sites; in fact, the E600Q mutation in rat TRPV1 enhanced the potentiation effect (Ahern et al., 2006). Gd^{3+} appears to indeed bind to the proton-binding sites, as it competes with H^+ (Tousova et al., 2005).

Interaction between divalent cations and ion channels has been observed previously in many channel types. In most cases, Mg^{2+} of physiological concentrations (low millimolar) enters the channel pore to block ion flux, causing current rectification of the inward-rectifying potassium channels (Horie et al., 1987; Ciani and Ribalet, 1988) and current inhibition of the NMDA receptors (Nowak et al., 1984) and calcium channels (Lansman et al., 1986). In this study, we observed a similar conductance inhibition by Mg^{2+} in TRPV1. Mg^{2+} is found to also interact with the gating machinery of many channel types. In the case of ether-à-go-go channels, Mg^{2+} can substantially slow down channel activation kinetics (Terlau et al., 1996). The gating effect is voltage dependent and interestingly also involves competition between Mg^{2+} and H^+ for common binding sites, which were later identified to be aspartate residues in the S2 and S3 segments (Silverman et al., 2000; Tang et al., 2000). Mg^{2+} can exert a substantial gating effect on ether-à-go-go channel gating at submillimolar concentrations. Because TRPV1 protein contains many charged (both positive and negative) residues that are likely exposed to the extracellular side (including the two H^+-binding glutamates), it is possible that Mg^{2+} can potentially interact with them to exert a gating effect.

As mentioned earlier, ionic strength has been shown to be able to exert a strong influence on protein stability and conformational change. Given that divalent cations and other molecules with varying chemical natures generally exert similar potentiation effects that are observable only at 10–100-mM concentrations (Riera et al., 2007; Ohta et al., 2008), it is also possible that they may potentiate heat activation not by binding to specific channel sites. Instead, high concentrations of divalent cations in solution may have a global (or perhaps localized) effect on channel protein stability. Through this nonspecific interaction, Mg^{2+} and Ba^{2+} contribute a favorable energetic effect on heat activation. The observation that widespread extracellular structures mediate the gating effect of divalent cations is consistent with

this view. In a general sense, the process induced by high concentrations of divalent cations is not unlike protein denature induced by molar concentrations of urea. However, it is unlikely and unnecessary that complete denaturing of any part of the channel protein would occur during Mg^{2+}- and Ba^{2+}-induced activation. Instead, the gating machinery of TRPV1 shifts to a conformation that is normally unfavorable but becomes favorable at higher temperatures or in the presence of extracellular divalent cations.

In summary, widely spread extracellular structures are required for divalent cations to promote TRPV1 heat activation. Intracellular structures, however, are not involved in the potentiation process. As Mg^{2+}-induced turret movement precedes channel activation, it seems most likely that extracellular conformational rearrangement is coupled to the activation machinery and serves as the cause of channel activation rather than a coincidental or accommodating structural adjustment.

REFERENCES

Ahern, G.P., I.M. Brooks, R.L. Miyares, and X.B. Wang. 2005. Extracellular cations sensitize and gate capsaicin receptor TRPV1 modulating pain signaling. *J. Neurosci.* 25:5109–5116. http://dx.doi.org/10.1523/JNEUROSCI.0237-05.2005

Ahern, G.P., X. Wang, and R.L. Miyares. 2006. Polyamines are potent ligands for the capsaicin receptor TRPV1. *J. Biol. Chem.* 281:8991–8995. http://dx.doi.org/10.1074/jbc.M513429200

Bezanilla, F. 2008. How membrane proteins sense voltage. *Nat. Rev. Mol. Cell Biol.* 9:323–332. http://dx.doi.org/10.1038/nrm2376

Boukalova, S., J. Teisinger, and V. Vlachova. 2013. Protons stabilize the closed conformation of gain-of-function mutants of the TRPV1 channel. *Biochim. Biophys. Acta.* 1833:520–528. http://dx.doi.org/10.1016/j.bbamcr.2012.11.017

Bykova, E.A., X.D. Zhang, T.Y. Chen, and J. Zheng. 2006. Large movement in the C terminus of CLC-0 chloride channel during slow gating. *Nat. Struct. Mol. Biol.* 13:1115–1119. http://dx.doi.org/10.1038/nsmb1176

Cao, X., L. Ma, F. Yang, K. Wang, and J. Zheng. 2013. Divalent cations potentiate TRPV1 channel by lowering the heat activation threshold. *J. Gen. Physiol.* 143:75–90.

Cheng, W., F. Yang, C.L. Takanishi, and J. Zheng. 2007. Thermosensitive TRPV channel subunits coassemble into heteromeric channels with intermediate conductance and gating properties. *J. Gen. Physiol.* 129:191–207. http://dx.doi.org/10.1085/jgp.200709731

Ciani, S., and B. Ribalet. 1988. Ion permeation and rectification in ATP-sensitive channels from insulin-secreting cells (RINm5F): effects of K^+, Na^+ and Mg^{2+}. *J. Membr. Biol.* 103:171–180. http://dx.doi.org/10.1007/BF01870947

Clapham, D.E., and C. Miller. 2011. A thermodynamic framework for understanding temperature sensing by transient receptor potential (TRP) channels. *Proc. Natl. Acad. Sci. USA.* 108:19492–19497. http://dx.doi.org/10.1073/pnas.1117485108

Cui, Y., F. Yang, X. Cao, V. Yarov-Yarovoy, K. Wang, and J. Zheng. 2012. Selective disruption of high sensitivity heat activation but not capsaicin activation of TRPV1 channels by pore turret mutations. *J. Gen. Physiol.* 139:273–283. http://dx.doi.org/10.1085/jgp.201110724

Erickson, M.G., B.A. Alseikhan, B.Z. Peterson, and D.T. Yue. 2001. Preassociation of calmodulin with voltage-gated Ca^{2+} channels revealed by FRET in single living cells. *Neuron.* 31:973–985. http://dx.doi.org/10.1016/S0896-6273(01)00438-X

Fersht, A. 1998. Structure and Mechanism in Protein Science: A Guide to Enzyme Catalysis and Protein Folding. W.H. Freeman and Company, New York. 650 pp.

Grandl, J., S.E. Kim, V. Uzzell, B. Bursulaya, M. Petrus, M. Bandell, and A. Patapoutian. 2010. Temperature-induced opening of TRPV1 ion channel is stabilized by the pore domain. *Nat. Neurosci.* 13:708–714. http://dx.doi.org/10.1038/nn.2552

Gyires, K., and Z. Torma. 1984. The use of the writhing test in mice for screening different types of analgesics. *Arch. Int. Pharmacodyn. Ther.* 267:131–140.

Horie, M., H. Irisawa, and A. Noma. 1987. Voltage-dependent magnesium block of adenosine-triphosphate-sensitive potassium channel in guinea-pig ventricular cells. *J. Physiol.* 387:251–272.

Islas, L.D., and F.J. Sigworth. 2001. Electrostatics and the gating pore of Shaker potassium channels. *J. Gen. Physiol.* 117:69–90. http://dx.doi.org/10.1085/jgp.117.1.69

Jordt, S.E., M. Tominaga, and D. Julius. 2000. Acid potentiation of the capsaicin receptor determined by a key extracellular site. *Proc. Natl. Acad. Sci. USA.* 97:8134–8139. http://dx.doi.org/10.1073/pnas.100129497

Lansman, J.B., P. Hess, and R.W. Tsien. 1986. Blockade of current through single calcium channels by Cd^{2+}, Mg^{2+}, and Ca^{2+}. Voltage and concentration dependence of calcium entry into the pore. *J. Gen. Physiol.* 88:321–347. http://dx.doi.org/10.1085/jgp.88.3.321

Lee, S.Y., A. Banerjee, and R. MacKinnon. 2009. Two separate interfaces between the voltage sensor and pore are required for the function of voltage-dependent K^+ channels. *PLoS Biol.* 7:e47. http://dx.doi.org/10.1371/journal.pbio.1000047

Long, S.B., E.B. Campbell, and R. Mackinnon. 2005. Crystal structure of a mammalian voltage-dependent Shaker family K^+ channel. *Science.* 309:897–903. http://dx.doi.org/10.1126/science.1116269

Long, S.B., X. Tao, E.B. Campbell, and R. MacKinnon. 2007. Atomic structure of a voltage-dependent K^+ channel in a lipid membrane-like environment. *Nature.* 450:376–382. http://dx.doi.org/10.1038/nature06265

Luebbert, M., D. Radtke, R. Wodarski, N. Damann, H. Hatt, and C.H. Wetzel. 2010. Direct activation of transient receptor potential V1 by nickel ions. *Pflugers Arch.* 459:737–750. http://dx.doi.org/10.1007/s00424-009-0782-8

Mogil, J.S., S.G. Wilson, K. Bon, S.E. Lee, K. Chung, P. Raber, J.O. Pieper, H.S. Hain, J.K. Belknap, L. Hubert, et al. 1999. Heritability of nociception I: responses of 11 inbred mouse strains on 12 measures of nociception. *Pain.* 80:67–82. http://dx.doi.org/10.1016/S0304-3959(98)00197-3

Moiseenkova-Bell, V.Y., L.A. Stanciu, I.I. Serysheva, B.J. Tobe, and T.G. Wensel. 2008. Structure of TRPV1 channel revealed by electron cryomicroscopy. *Proc. Natl. Acad. Sci. USA.* 105:7451–7455. http://dx.doi.org/10.1073/pnas.0711835105

Myers, B.R., C.J. Bohlen, and D. Julius. 2008. A yeast genetic screen reveals a critical role for the pore helix domain in TRP channel gating. *Neuron.* 58:362–373. http://dx.doi.org/10.1016/j.neuron.2008.04.012

Neyton, J., and C. Miller. 1988. Potassium blocks barium permeation through a calcium-activated potassium channel. *J. Gen. Physiol.* 92:549–567. http://dx.doi.org/10.1085/jgp.92.5.549

Nowak, L., P. Bregestovski, P. Ascher, A. Herbet, and A. Prochiantz. 1984. Magnesium gates glutamate-activated channels in mouse central neurones. *Nature.* 307:462–465. http://dx.doi.org/10.1038/307462a0

Ohta, T., T. Imagawa, and S. Ito. 2008. Novel gating and sensitizing mechanism of capsaicin receptor (TRPV1): tonic inhibitory regulation of extracellular sodium through the external protonation sites on TRPV1. *J. Biol. Chem.* 283:9377–9387. http://dx.doi.org/10.1074/jbc.M709377200

Piasta, K.N., D.L. Theobald, and C. Miller. 2011. Potassium-selective block of barium permeation through single KcsA channels. *J. Gen. Physiol.* 138:421–436. http://dx.doi.org/10.1085/jgp.201110684

Riera, C.E., H. Vogel, S.A. Simon, and J. le Coutre. 2007. Artificial sweeteners and salts producing a metallic taste sensation activate TRPV1 receptors. *Am. J. Physiol. Regul. Integr. Comp. Physiol.* 293:R626–R634. http://dx.doi.org/10.1152/ajpregu.00286.2007

Sigworth, F.J. 1994. Voltage gating of ion channels. *Q. Rev. Biophys.* 27:1–40. http://dx.doi.org/10.1017/S0033583500002894

Silverman, W.R., C.Y. Tang, A.F. Mock, K.B. Huh, and D.M. Papazian. 2000. Mg^{2+} modulates voltage-dependent activation in ether-à-go-go potassium channels by binding between transmembrane segments S2 and S3. *J. Gen. Physiol.* 116:663–678. http://dx.doi.org/10.1085/jgp.116.5.663

Takanishi, C.L., E.A. Bykova, W. Cheng, and J. Zheng. 2006. GFP-based FRET analysis in live cells. *Brain Res.* 1091:132–139. http://dx.doi.org/10.1016/j.brainres.2006.01.119

Tang, C.Y., F. Bezanilla, and D.M. Papazian. 2000. Extracellular Mg^{2+} modulates slow gating transitions and the opening of *Drosophila* ether-à-go-go potassium channels. *J. Gen. Physiol.* 115:319–338. http://dx.doi.org/10.1085/jgp.115.3.319

Terlau, H., J. Ludwig, R. Steffan, O. Pongs, W. Stühmer, and S.H. Heinemann. 1996. Extracellular Mg^{2+} regulates activation of rat eag potassium channel. *Pflugers Arch.* 432:301–312. http://dx.doi.org/10.1007/s004240050137

Tominaga, M., M.J. Caterina, A.B. Malmberg, T.A. Rosen, H. Gilbert, K. Skinner, B.E. Raumann, A.I. Basbaum, and D. Julius. 1998. The cloned capsaicin receptor integrates multiple pain-producing stimuli. *Neuron.* 21:531–543. http://dx.doi.org/10.1016/S0896-6273(00)80564-4

Tousova, K., L. Vyklicky, K. Susankova, J. Benedikt, and V. Vlachova. 2005. Gadolinium activates and sensitizes the vanilloid receptor TRPV1 through the external protonation sites. *Mol. Cell. Neurosci.* 30:207–217. http://dx.doi.org/10.1016/j.mcn.2005.07.004

Voets, T., G. Droogmans, U. Wissenbach, A. Janssens, V. Flockerzi, and B. Nilius. 2004. The principle of temperature-dependent gating in cold- and heat-sensitive TRP channels. *Nature.* 430:748–754. http://dx.doi.org/10.1038/nature02732

Wang, S., K. Poon, R.E. Oswald, and H.H. Chuang. 2010. Distinct modulations of human capsaicin receptor by protons and magnesium through different domains. *J. Biol. Chem.* 285:11547–11556. http://dx.doi.org/10.1074/jbc.M109.058727

Yang, F., Y. Cui, K. Wang, and J. Zheng. 2010. Thermosensitive TRP channel pore turret is part of the temperature activation pathway. *Proc. Natl. Acad. Sci. USA.* 107:7083–7088. http://dx.doi.org/10.1073/pnas.1000357107

Zheng, J. 2013a. Domain–domain interactions in ion channels. *J. Gen. Physiol.* 142:347–350. http://dx.doi.org/10.1085/jgp.201311090

Zheng, J. 2013b. Molecular mechanism of TRP channels. *Compr Physiol.* 3:221–242.

Zheng, J., and W.N. Zagotta. 2000. Gating rearrangements in cyclic nucleotide-gated channels revealed by patch-clamp fluorometry. *Neuron.* 28:369–374. http://dx.doi.org/10.1016/S0896-6273(00)00117-3

Zheng, J., M.C. Trudeau, and W.N. Zagotta. 2002. Rod cyclic nucleotide-gated channels have a stoichiometry of three CNGA1 subunits and one CNGB1 subunit. *Neuron.* 36:891–896. http://dx.doi.org/10.1016/S0896-6273(02)01099-1